

Chemical differentiation along the CepA-East outflows

C. Codella,¹ R. Bachiller,² M. Benedettini,^{3,4} P. Caselli,⁵ S. Viti⁴ and V. Wakelam^{6,7}

¹*Istituto di Radioastronomia, INAF, Sezione di Firenze, Largo E. Fermi 5, 50125 Firenze, Italy*

²*Observatorio Astronómico Nacional (IGN), Apartado 1143, E-28800, Alcalá de Henares (Madrid), Spain*

³*Istituto di Fisica dello Spazio Interplanetario, INAF, Area di Ricerca Tor Vergata, Via Fosso del Cavaliere 100, 00133 Roma, Italy*

⁴*Department of Physics and Astronomy, University College London, Gower Street WC1E6 BT London, UK*

⁵*Osservatorio Astrofisico di Arcetri, INAF, Largo E. Fermi 5, 50125 Firenze, Italy*

⁶*Observatoire de Bordeaux, BP 89, 33270 Floirac, France*

⁷*The Ohio State University, Department of Physics, 174 W. 18th Ave., Columbus, OH 43210-1106 USA*

Accepted date. Received date; in original form date

ABSTRACT

We present the results of a multiline survey at mm-wavelengths of the Cepheus A star forming region. Four main flows have been identified: three pointing in the SW, NE, and SE directions and accelerating high density CS clumps. The fourth outflow, revealed by high-sensitivity HDO observations, is pointing towards South and is associated with conditions particularly favourable to a chemical enrichment. At the CepA-East position the emissions due to the ambient clump and to the outflows coexist and different molecules exhibit different spectral behaviours. Some species (C^{13}CH , C_3H_2 , CH_2CO , $\text{CH}_3\text{C}_2\text{H}$, HC^{18}O^+) exhibit relatively narrow lines at ambient velocities (ambient peak). Other molecules (CO , CS , H_2S , SiO , SO , SO_2) show extended wings tracing the whole range of the outflow velocities. Finally, OCS , H_2CS , HDO , and CH_3OH are associated with wings and, in addition, show wings and in addition reveal a bright high velocity redshifted spectral peak (outflow peak) which can be used to investigate the southern outflows. At ambient velocities the gas is dense ($> 10^5 \text{ cm}^{-3}$) and different components at distinct temperatures coexist, ranging from the relatively low kinetic temperatures ($\leq 50 \text{ K}$) measured with H_2S , CH_3OH , H_2CS , and $\text{CH}_3\text{C}_2\text{H}$, to definitely higher temperature conditions, $\sim 100\text{--}200 \text{ K}$, obtained from the SiO , SO , and SO_2 spectra. For the outflow peak we derive densities between $\sim 10^4 \text{ cm}^{-3}$ to $\sim 10^7 \text{ cm}^{-3}$ and high temperatures, $\simeq 100\text{--}200 \text{ K}$, indicating regions compressed and heated by shocks.

The analysis of the line profiles shows that the SiO molecule dominates at the highest velocities and at the highest excitation conditions, confirming its close association with shocks. H_2S , SO_2 , and SO preferentially trace more quiescent regions than SiO , and in particular a lack of bright H_2S emission at the highest velocities is found. OCS and H_2CS emit at quite high velocities, where the abundances of three shock tracers like SiO , CH_3OH , and HDO are higher. These results may indicate that H_2S is not the only major sulphur carrier in the grain mantles, and that OCS and H_2CS may probably play an important role on the grains; or that alternatively they rapidly form once the mantle is evaporated after the passage of a shock. Finally, the outflow peak emission has been compared with recent time-dependent sulphur chemistry models: the results indicate that, if associated with accurate measurements of the physical conditions, the $\text{CH}_3\text{OH}/\text{H}_2\text{CS}$ column density ratio can be used as an effective chemical clock to date the age of shocked gas.

Key words: ISM: clouds – ISM: individual objects: CepA – ISM: jets and outflows – ISM: molecules – Radio lines: ISM

1 INTRODUCTION

The mass loss from Young Stellar Objects (YSOs) produces high velocity flows which strike the ambient medium driv-

ing shocks. Once the temperature has increased, at least to a few thousands degrees depending on the shock type, the energy barriers between neutral molecules can be over-

come and the chemistry of certain species, such as the sulphuretted species, is altered significantly (see e.g. Pineau des Forêts et al. 1993, van Dishoeck & Blake 1998, and reference therein). In addition, grains are affected by shocks, with the consequent injection of molecular and atomic species in the gas phase: again, this leads to an enhancement of the abundances of several species, including S-bearing molecules. The scenario proposed by most models is that H_2S is the main reservoir of sulphur on grain mantles: once in the gas phase, H_2S is used for a fast production of SO and SO_2 (e.g. Pineau des Forêts et al. 1993, Charnley 1997). However, the lack of H_2S features in the ISO spectra (Gibb et al. 2000, Boogert et al. 2000) which set upper limits on the iced H_2S abundance around protostars and the detection of OCS on grains (Palumbo et al. 1997) suggest that the latter may be an important sulphur carrier in the ices. This seems supported by the observations in the envelopes of massive young stars recently performed by van der Tak et al. (2003), which indicate for OCS higher excitation temperatures than for H_2S . An alternative hypothesis is that the sulphur released from the dust mantles is mainly in atomic form (Wakelam et al. 2004). In any case, once the gas phase has been enriched by the passage of a shock, other S-bearing species such as H_2CS and HCS^+ are expected to significantly increase their abundances as a consequence of the sulphur injection. Therefore, estimates of abundance ratios such as $\text{SO}_2/\text{H}_2\text{S}$, $\text{H}_2\text{S}/\text{OCS}$, and $\text{H}_2\text{CS}/\text{OCS}$ may provide us with chemical clocks to study the evolutionary stages of molecular outflows. In fact, the use of $\text{SO}_2/\text{H}_2\text{S}$ and $\text{H}_2\text{S}/\text{OCS}$ ratios has already led crude age estimates of the outflows located in CB3 (Codella & Bachiller 1999) and L1157 (Bachiller et al. 2001), encouraging further studies.

The high temperature scenario can be applied also to hot cores around protostars, which are characterised by high temperatures (≥ 100 K), high densities ($\geq 10^6$ cm $^{-3}$), and a rich molecular inventory. The $\text{SO}_2/\text{H}_2\text{S}$ ratio has been used by Hatchell et al. (1998) for massive hot cores: the inferred ages are in agreement with the dynamical times estimated from the associated outflows. Moreover, Buckle & Fuller (2003) show that the chemical evolution of sulphuretted species is a potential probe of timescales also in low-mass star forming regions. In summary, the effect of high-temperature chemistry on the composition of the gas hosting the star forming process can be used as a tool to investigate the evolution of protostars.

Physical conditions as well as time evolution affect the sulphur chemistry in high-temperatures environment. For instance, recently Wakelam et al. (2004) modeled the sulphur chemistry around hot core-like environments and found that the obtained abundances depend not only on age but also on the excitation conditions of the gas. Thus, in order to use the sulphur abundance ratios as chemical clocks, care should be taken to first constrain the gas conditions. In the case of molecular outflows, it is reasonable to expect different physical and/or chemical conditions at the different velocities and thus a study of the excitation as a function of the velocity is needed. The existing observations of sulphuretted molecules have been carried out to date in a unsystematic way, and, in particular, since the wing profiles are weak, the chemical composition of the gas at high-velocity has been poorly investigated. With this in mind, we carried out line observations of S-bearing species at mm-wavelengths to-

wards a star forming region with well defined high-velocity components. Cepheus A (CepA) well represents such target: in particular, the East component harbours an OB3 stellar association (Goetz et al. 1998, and references therein) driving multiple outflows (e.g. Narayanan & Walker 1996, Bergin et al. 1997). Bergin et al. (1997) have studied the chemical properties of Cepheus A showing that a large number of molecules can be easily detected, but their observations only trace the quiescent gas, this is likely due to the limitation in spatial and spectral resolutions, which does not allow the detection of the high velocity wings.

In this paper, we report the results of a deep millimeter survey of molecular lines in CepA. In particular, we compare line observations of SO, HCS^+ , H_2CS , OCS, H_2S , and SO_2 with profiles due to standard tracers of shocked gas, high excitation conditions, and of ambient emission. The main aim is to study the variation of the abundance ratios and the excitation conditions of S-bearing species along the line profiles. We find that sulphuretted molecules may be good chemical clocks to date molecular outflows and their driving protostellar sources.

2 OBSERVATIONS AND RESULTS

The observations were performed with the IRAM 30-m telescope at Pico Veleta (Granada, Spain) in June 2001, September 2002, August 2003, and June 2004. The observed molecular species, the transitions, their upper level energies, the Einstein A coefficients and rest frequencies and some observing parameters, such as the HPBW and the typical system temperature (T_{sys}) are summarised in Table 1. The integration time (ON+OFF source) ranged from about 1 to ~ 18 hours, depending on the intensities of the observed lines. The main beam efficiency varies from about 0.8 (at 81 GHz) to 0.5 (at 262 GHz). The observations were made by position switching. The pointing was checked about every hour by observing nearby planets or continuum sources and it was found to be accurate to within $4''$. As spectrometers, an autocorrelator (AC) split into different parts (up to six) was used to allow simultaneous observations of four different transitions. Also a 1 MHz filter bank, split into four parts of 256 channels, was simultaneously used. The velocity resolutions provided by both backends, AC and 1 MHz, are shown in Table 1. When considered convenient, the AC spectra were smoothed to a lower velocity resolution (up to ~ 1 km s $^{-1}$). The spectra were calibrated with the standard chopper wheel method and are reported here in units of main-beam brightness temperature (T_{MB}).

The multiline molecular survey has been performed towards CepA-East and, in particular, at the coordinates of the HW2 object, which is one of the YSOs thought to drive the molecular outflows: $\alpha_{2000} = 22^{\text{h}} 56^{\text{m}} 17^{\text{s}}.9$, $\delta_{2000} = +62^{\circ} 01' 49''.7$. In addition, we present maps of CepA-East in CS, a well known tracer of high density clumps, and in HDO, which traces hot gas chemistry as well as shocked material (e.g. van Dishoeck & Blake 1998). In particular, the heavy water emission will be here used as alternative to H_2O , whose observations are prevented from the ground due to very strong atmospheric absorption. Water is expected to be one of the most important coolant in non-dissociative shocks (e.g. Kaufman & Neufeld 1996), since its gas-phase

Table 1. List of molecular species, transitions and observing parameters

Transition	ν_0 (MHz)	E_u (K)	A_{ul} (s ⁻¹)	F_{int} (K km/s)	HPBW ($''$)	T_{sys} (K)	$dv(\text{AC})$ (km/s)	$dv(1\text{MHz})$ (km/s)
Selected transitions								
HDO($J_{K_-K_+} = 1_{10-1_{11}}$)	80578.30	47	1.3×10^{-6}	0.58(0.05)	31	150	0.15	3.72
OCS($J = 7-6$)	85139.12	16	1.7×10^{-6}	0.36(0.02)	29	110	0.14	–
HCS ⁺ ($J = 2-1$)	85347.88	6	1.1×10^{-5}	0.38(0.04)	29	110	0.14	3.51
CH ₃ C ₂ H($J_K = 5_K-4_K$)	85457.30 ^a	12 ^a	2.0×10^{-6a}	$3.11(0.13)^b$	29	150	0.27	3.51
C ³⁴ S($J = 2-1$)	96412.98	7	1.6×10^{-5}	2.16(0.18)	26	220	0.24	3.11
CS($J = 2-1$)	97980.97	7	1.7×10^{-5}	28.03(0.14)	25	180	0.24	3.06
SO($J_K = 3_2-2_1$)	99299.88	4	1.1×10^{-5}	14.42(0.03)	24	150	0.24	3.02
H ₂ CS($J_{K_-K_+} = 3_{13}-2_{12}$)	101477.75	23	1.3×10^{-5}	1.01(0.03)	24	187	0.12	2.95
³⁴ SO ₂ ($J_{K_-K_+} = 3_{13}-2_{02}$)	102031.91	8	9.5×10^{-6}	0.11(0.01)	24	130	0.11	2.94
CH ₃ C ₂ H($J_K = 6_K-5_K$)	102547.98 ^a	17 ^a	3.4×10^{-6a}	$4.16(0.14)^b$	24	200	0.23	2.90
SO($J_K = 4_3-3_2$)	138178.64	9	3.1×10^{-5}	22.76(0.19)	17	370	0.17	2.17
CH ₃ OH($J_K = 3_K-2_K$)	145103.23 ^a	14 ^a	1.2×10^{-5a}	$5.64(0.15)^a$	17	280	0.08	2.07
H ₂ ³⁴ S($J_{K_-K_+} = 1_{10}-0_{10}$)	167910.52	28	2.6×10^{-5}	1.11(0.23)	14	480	0.07	1.79
H ₂ CS($J_{K_-K_+} = 6_{16}-5_{15}$)	202923.55	47	1.2×10^{-4}	2.15(0.08)	12	460	0.06	1.48
CH ₃ C ₂ H($J_K = 12_K-11_K$)	205080.73 ^a	64 ^a	2.8×10^{-5a}	$6.71(0.36)^b$	12	600	0.11	1.46
HCS ⁺ ($J = 5-4$)	213360.64	31	2.0×10^{-4}	0.59(0.08)	12	330	0.04	1.41
H ₂ ³⁴ S($J_{K_-K_+} = 2_{20}-2_{11}$)	213376.92	84	1.7×10^{-5}	$\leq 0.07^c$	12	330	0.04	1.41
SiO($J = 5-4$)	217104.94	31	5.2×10^{-4}	8.71(0.24)	11	450	0.43	1.38
C ¹⁸ O($J = 2-1$)	219560.33	16	6.2×10^{-7}	47.94(0.25)	11	580	0.43	1.36
SO($J_K = 6_5-5_4$)	219949.39	24	1.3×10^{-4}	40.74(0.30)	11	580	0.11	1.36
CO($J = 2-1$)	230537.98	17	6.9×10^{-7}	– ^d	10	1100	0.10	1.30
C ³⁴ S($J = 5-4$)	241016.17	34	2.8×10^{-4}	1.75(0.40)	10	990	0.10	1.24
HDO($J_{K_-K_+} = 2_{11}-2_{12}$)	241561.53	95	1.2×10^{-5}	3.42(0.19)	10	68	0.05	1.24
CH ₃ OH($J_K = 5_K-4_K$)	241791.44 ^a	35 ^a	5.8×10^{-5a}	$8.32(0.07)^a$	10	678	0.05	1.24
H ₂ CS($J_{K_-K_+} = 7_{16}-6_{15}$)	244047.75	60	2.1×10^{-4}	1.36(0.06)	10	890	0.05	1.23
CS($J = 5-4$)	244935.61	34	3.0×10^{-4}	47.33(0.53)	10	1100	0.10	1.22
SO($J_K = 7_6-6_5$)	261843.72	35	2.2×10^{-4}	52.30(0.58)	9	1300	0.09	1.15
Serendipity detections								
HC ¹⁸ O ⁺ ($J = 1-0$)	85162.21	4	3.6×10^{-5}	0.65(0.02)	29	110	0.14	–
C ¹³ CH($J_{K_-K_+} = 1_{11}-0_{11}$)	85307.69	4	1.3×10^{-6}	0.18(0.03)	29	110	–	3.51
C ₃ H ₂ ($J_{K_-K_+} = 2_{12}-1_{01}$)	85338.91	6	2.3×10^{-5}	1.18(0.05)	29	110	0.14	3.51
CH ₂ CO($J_{K_-K_+} = 5_{14}-4_{13}$)	101981.43	23	1.1×10^{-5}	0.14(0.01)	24	130	0.11	2.94
CH ₃ OH($J_K = 10_{-2}-10_1$ E)	102122.70	154	1.7×10^{-7}	0.08(0.01)	24	130	–	2.94
CH ₃ OH($J_K = 9_1-9_0$ E)	167931.13	126	2.3×10^{-5}	2.33(0.25)	14	480	0.07	1.79
CH ₃ OH($J_K = 13_6-14_5$ E)	213377.52	390	1.1×10^{-5}	0.43(0.03)	12	330	0.04	1.41
CH ₃ OH($J_K = 1_1-0_0$ E)	213427.12	13	3.4×10^{-5}	2.20(0.06)	12	330	0.04	1.41
³⁴ SO ₂ ($J_{K_-K_+} = 16_{115}-15_{214}$)	241509.05	131	8.3×10^{-5}	0.78(0.14)	10	670	–	1.24
HNCO($J_{K_-K_+} = 11_{011}-10_{010}$)	241774.09	58	2.0×10^{-4}	2.81(0.20)	10	678	0.05	1.24
³⁴ SO ₂ ($J_{K_-K_+} = 18_{117}-18_{018}$)	243935.88	163	7.0×10^{-5}	0.61(0.73)	10	890	–	1.23

^a For CH₃OH, it refers to the J_0-J_{-10} A⁺ line, while for CH₃C₂H it refers to the $K=0$ component. ^b For CH₃C₂H the integrated flux refers to the $K=0,1$ pattern. ^c It refers to the 3σ noise level; ^d The CO(2–1) observations have been performed in wobbler mode losing the information at ambient velocities in order to investigate the high-velocity wings.

abundance is considerably enhanced both via high temperature (larger than 200–300 K) reactions and by sputtering. Given the characteristics of CepA-East, it will thus be possible to examine in details how the dense medium is affected by the occurrence of YSOs

Table 1 reports the selected transitions and their flux F_{int} (K km s⁻¹) integrated along the whole profile: all but H₂³⁴S(2₂₀–2₁₁) have been detected. The maps of CepA in H₂S(1₁₀–1₀₁, 2₂₀–2₁₁) and SO₂(3₁₃–2₀₂, 5₂₄–4₁₃, 16₂₁₄–15₃₁₃) had been already reported in a previous paper (Codella et al. 2003). The results indicate the occurrence of a rich chemistry associated with CepA-East, confirming the

findings of Bergin et al. (1997). The gas surrounding this region is particularly rich in the S-bearing molecules (SO, H₂S, SO₂, H₂CS, HCS⁺, OCS). Also line spectra due to tracers of the high density clumps hosting the YSOs (CS, C¹⁸O, and CH₃C₂H) as well as to tracers of hot and/or shocked material (SiO, HDO, CH₃OH) have been obtained. Moreover, the use of large bandwidths allowed us to serendipitously detect a number of other emission lines due to HC¹⁸O⁺, C₃H₂, C¹³CH, CH₂CO, CH₃OH, and HNCO, as shown in the lower part of Tab. 1. Table 2 reports the lines which have not been identified, listing the observed peak frequency, the

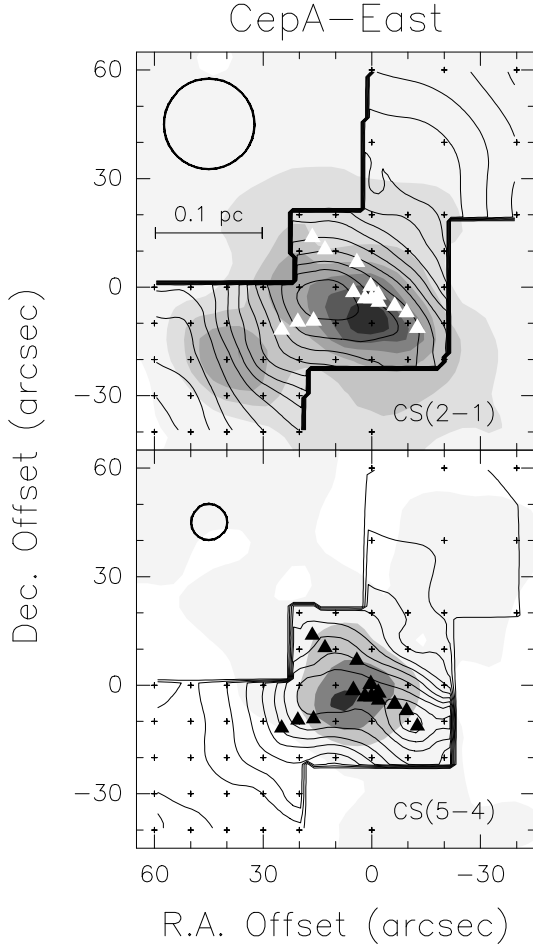


Figure 1. Contour maps of the integrated CS $J=2-1$ (upper panel) and $J=5-4$ (lower panel) integrated emission towards CepA-East. The maps are overlaid with the grey scale images reproducing the integrated emission of $\text{H}_2^{32}\text{S}(1_{10}-1_{01})$ (upper panel) and $^{32}\text{SO}_2(3_{13}-2_{02})$ (lower panel), reported by Codella et al. (2003) in their Fig. 1. The empty circles show the IRAM beam (HPBW), while the small crosses mark the observed positions. The triangles stand for the VLA 2 cm continuum components which trace in the East region two strings of sources arising in shocks (Garay et al. 1996). The velocity integration interval is $-30, +10 \text{ km s}^{-1}$. The contours range from 1.0 to 31.0 K km s^{-1} (upper panel) and from 3.0 to 57.0 K km s^{-1} (lower panel). The first contours and the steps correspond to about 3 and 6 σ , respectively (where σ is the r.m.s. of the map).

spectral resolution, the peak temperature and the FWHM linewidth.

Table 1 shows that the lines detected are associated with a wide range of excitation, from few to hundreds of Kelvins. In particular, the detection of emission due to transitions above 100 K clearly suggest the presence of high temperature conditions, which could be associated to the presence of a hot core and/or the occurrence of shocked material, and consequently requires the analysis of the maps and of the line profiles.

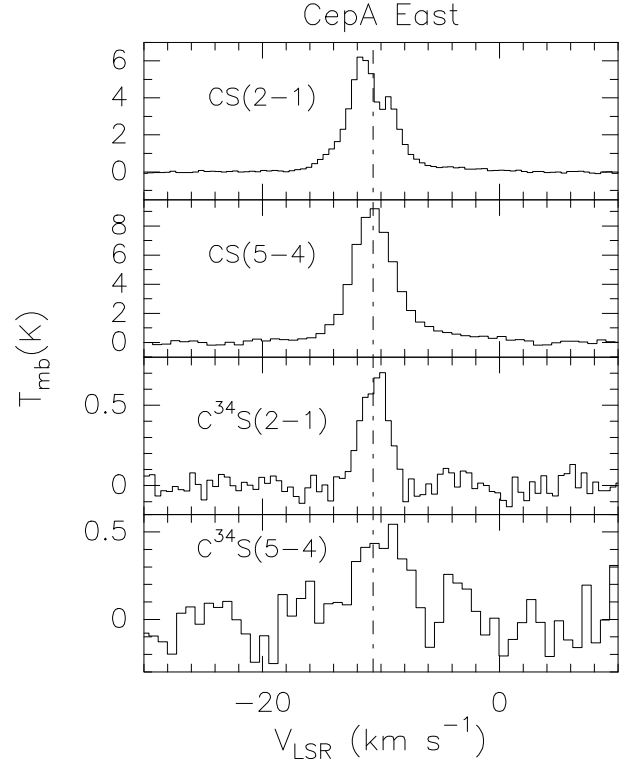


Figure 2. CS and C^{34}S line profiles observed towards CepA East: transitions are reported. The dashed line stands for the ambient LSR velocity (-10.65 km s^{-1}), according to the CS $J=5-4$ and $\text{C}^{18}\text{O } J=2-1$ measurement (see text).

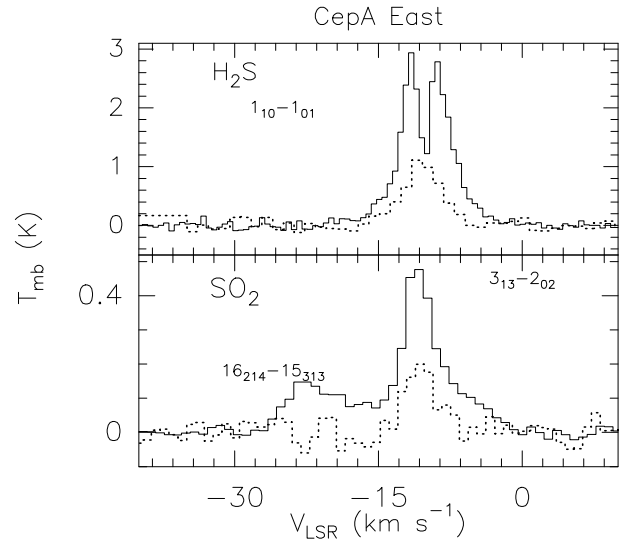


Figure 3. CepA East: comparison between same line transitions of different isotopomers. The solid lines are for the $\text{H}_2^{32}\text{S}(1_{10}-1_{01})$ and $^{32}\text{SO}_2(3_{13}-2_{02})$ profiles reported by Codella et al. (2003). The dotted lines show the corresponding H_2^{34}S and $^{34}\text{SO}_2$ spectra, rescaled to be comparable with the ^{32}S -lines. Note that only for $^{32}\text{SO}_2$, the $3_{13}-2_{02}$ line is blended with the $16_{214}-15_{313}$ emission.

Table 2. Unidentified detections observed towards CepA-East

Obs. frequency (MHz)	$d\nu$ (MHz)	T_{MB} (mK)	$FWHM$ (km/s)
U-102062.23(0.15)	0.31	15(3)	7.8(2.1)
U-202811.00(0.19)	1.00	96(20)	5.3(0.9)
U-213303.65(0.14)	1.00	101(12)	8.4(1.6)
U-216758.40(0.47)	1.00	80(19)	9.5(1.8)

3 A VIEW OF CEPA-EAST: DENSE CLUMPS AND OUTFLOWS

3.1 Ambient emission

We produced relatively small CS maps of CepA-East in order to carefully study the distribution of the ambient clumps. In particular, we focused our attention on the regions where the two strings of VLA continuum sources associated with shocks (Garay et al. 1996) and the H₂S and SO₂ clumps (Codella et al. 2003) are located. Figure 1 shows the maps of the integrated emission due to CS $J=2-1$ (upper panel) and $J=5-4$ (lower panel) and compare such distributions with those of H₂S $J_{K-K_+} = 1_{10}-1_{01}$ (upper panel) and SO₂ $J_{K-K_+} = 3_{13}-2_{02}$ (lower panel), reported in gray scale. The triangles stand for the VLA objects. It is possible to note that the two CS maps peak at different positions, probably due to the self-absorption of the 2-1 line (see the self-reversed profile in Fig. 2). Also the H₂S and SO₂ emissions show a different distribution with respect to CS, indicating that such molecules are not simply reproducing the same gas distribution and are able to trace different gas associated with different physical and/or chemical conditions.

Figure 2 reports the CS (upper panels) and C³⁴S (lower panels) spectra due to the $J=2-1$ and $5-4$ transitions. Although the CS(5-4) line shows the occurrence of wings which modify the gaussian profile at about 15% of the line peak, such emission can be used to define the characteristics of the ambient emission: the LSR velocity is -10.65 km s^{-1} (dashed line in Fig. 2), while the FWHM is 3.8 km s^{-1} . The comparison between these CS spectra confirms what found in the recent paper by Bottinelli & Williams (2004) which clearly indicates that the CS(2-1) profile is affected by self-absorption, whereas the CS(5-4) and the two transitions of C³⁴S, due to higher excitation and/or smaller abundance, are definitely optically thinner and thus well centered at the LSR ambient velocity. Moreover, as reported also by Bottinelli & Williams (2004), the CS(2-1) line shows a blueshifted peak brighter than the redshifted one, suggesting that infall motions can play an important role in the dynamics of the material traced by CS.

Figure 3 compares the H₂³⁴S($1_{10}-1_{01}$) and the ³⁴SO₂($3_{13}-2_{02}$) spectra (dotted lines, see also Fig. 1) with the profiles of the main isotopomers (continuous lines), reported in a previous paper (Codella et al. 2003). Note that the SO₂($3_{13}-2_{02}$) profile is blended with the $16_{214}-15_{313}$ line. The comparison between the H₂S spectra indicates that the double-peak H₂³²S pattern is caused by self-absorption, with the H₂³⁴S line peaking at the LSR velocity, where H₂³²S shows the relative minimum. On the other hand, Fig. 3 confirms that the detected SO₂ lines do not present self-absorption effects and they peak at the ambient velocity.

3.2 Kinematics

Figure 1 shows an elongated structure oriented in the NE-SW direction in the CS(5-4) line, which is not affected by self-absorption and it has been observed with an angular resolution of $10''$. To further study this distribution, a CS(5-4) channel map is reported in Fig. 4. Focusing the attention on the emission at velocities close to the ambient one, which corresponds to -10.7 with a FWHM of 1.8 km s^{-1} , we note that the elongated structure is due to the presence of two clumps centered respectively at the $(+20'', 0'')$ and $(-10'', -10'')$ offset map positions and with a beam deconvolved size of about $15''$ (0.05 pc at a distance of 725 pc , Sargent 1977) at slightly different velocities. This picture resembles the distribution of another high-density tracers such as N₂H⁺ (Bergin et al. 1997): the two clumps could indicate star forming sites or could point to gas components accelerated by the interaction with the mass loss processes indicated by the NE-SW VLA string. The latter case seems to be more likely since the clumps are symmetrically located with respect to the positions of the driving YSOs (the HW2 object is located at the centre of the map) and lie along the direction corresponding to the main axis of an extremely high-velocity outflow ($v-v_{\text{LSR}} \geq 20 \text{ km s}^{-1}$; e.g. Narayanan & Walker 1996).

On the other hand, from Fig. 4 it is possible to see (i) redshifted (up to -2 km s^{-1}) and blueshifted (up to -15 km s^{-1}) emission associated with the SW jet, and (ii) a blueshifted clump located at the end of the SE VLA chain as clearly reported in the -15 km s^{-1} panel. The latter clump is also seen in H₂S at high velocities (see Fig. 4 of Codella et al. 2003) and visible in Fig. 1 (upper panel) at $(+40'', -20'')$, confirming that at this position we are tracing high density material associated with outflow motions. In conclusion, the CS emission traces two outflow directions, the SW and SE ones, associated with two strings of shocked sources.

Figure 5 shows the contour maps of the $J_{K-K_+} = 1_{10}-1_{11}$, and $2_{11}-2_{12}$ integrated HDO emission towards CepA-East. In particular, considering the CS results, the southern region has also been mapped to look for signposts of outflow motions. The $1_{10}-1_{11}$ emission clearly indicates (i) a structure elongated along the SW direction with a peak near the centre of the map, and (ii) another elongated feature pointing towards South (see Sect. 3.3). On the other hand, the $2_{11}-2_{12}$ HDO map, obtained with higher resolution ($10''$), reveals a $\sim 15''$ (0.05 pc) clump centered at the HW2 coordinates, where the YSOs are located, and a second unresolved structure lying along the SW VLA jet.

In order to study the HDO kinematics, we present in Figures 6 and 7 the velocity channel maps of the $1_{10}-1_{11}$ and $2_{11}-2_{12}$ emissions, respectively. From these maps we argue that HDO in CepA-East traces the outflow activity as well as a small region around the driving YSOs. A quite complex scenario is therefore drawn: (i) a central component, clearly shown by the $2_{11}-2_{12}$ line, which is associated both with ambient velocity and higher redshifted (up to -2 km s^{-1}) velocities; (ii) a component associated with the SW VLA chain and emitting in both HDO lines and (iii) a final component pointing towards South and detected through the $1_{10}-1_{11}$ line. These last two components emit at redshifted velocities (up to -4 km s^{-1}) and at -12 and -11 km s^{-1} , i.e. at velocities close to the ambient one. Note that the -12 and

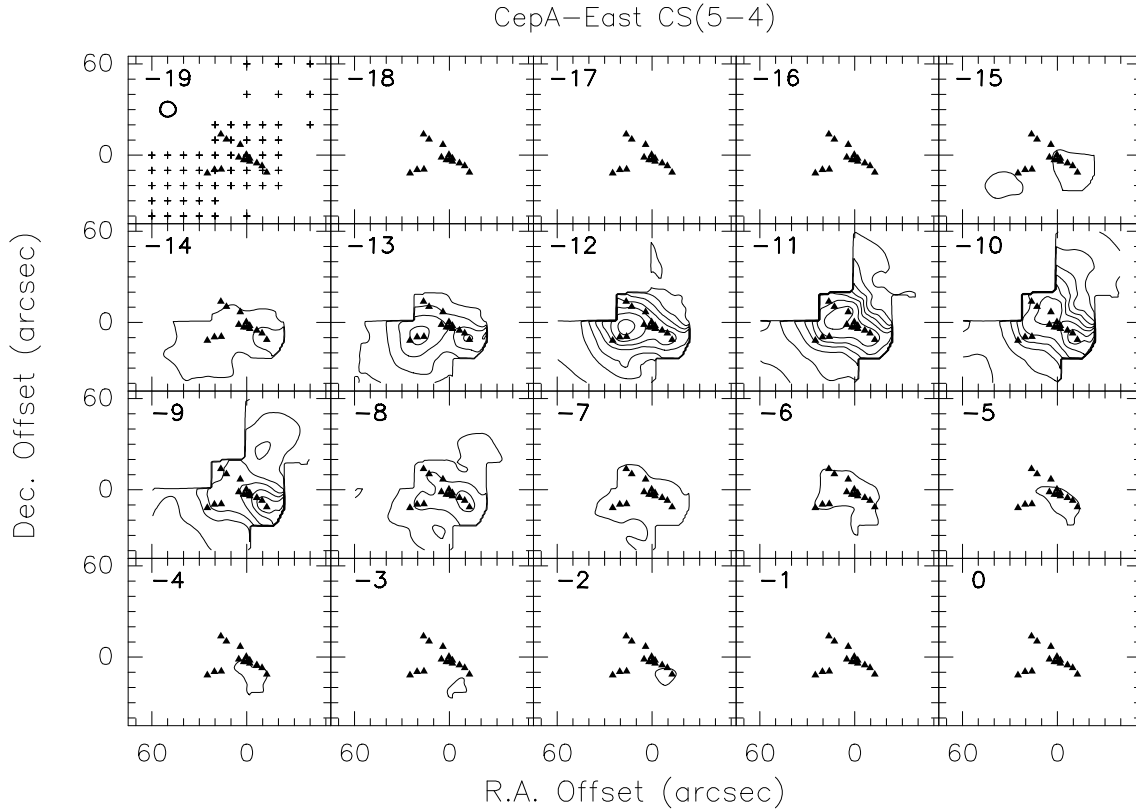


Figure 4. Channel map of the CS $J = 5-4$ emission towards CepA-East. Each panel shows the emission integrated over a velocity interval of 1 km s^{-1} centred at the value given in the left corner. Symbols are drawn as in Fig. 1. The ambient velocity emission is -10.7 km s^{-1} according to CS $J = 5-4$ and $\text{C}^{18}\text{O } J = 2-1$ measurements (see Sect. 3.2). The contours range from 0.75 ($\sim 5\sigma$) to 9.75 K km s^{-1} by step of 1.50 K km s^{-1} .

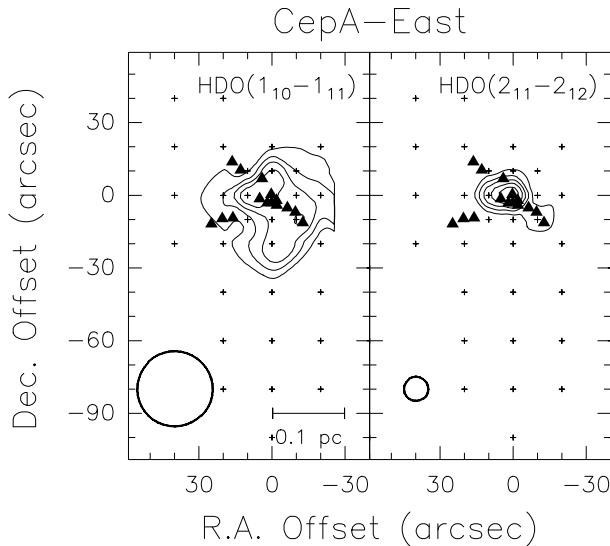


Figure 5. Contour maps of the integrated HDO $J_{K_{-}K_{+}} = 1_{10}-1_{11}$ (upper panel) and $J_{K_{-}K_{+}} = 2_{11}-2_{12}$ (lower panel) integrated emission towards CepA-East. Symbols are drawn as in Fig. 1. The velocity integration interval is $-20, 0 \text{ km s}^{-1}$. The contours range from 0.14 to 0.56 K km s^{-1} (upper panel) and from 0.60 to 3.00 K km s^{-1} (lower panel). The first contours and the steps correspond to about 3σ .

-11 km s^{-1} panels of Fig. 6 seem to indicate also the possible occurrence of a HDO $1_{10}-1_{11}$ clump at $(0'', -80'')$, along the southern direction, suggesting a connection with the central feature pointing towards South. This southern emission has not been detected with the $2_{11}-2_{12}$ line and therefore for the sake of clarity in the corresponding channel maps in Fig. 7 only a zoom of a smaller region is shown.

3.3 HDO and H₂S

In order to further investigate the southern molecular outflow, the present HDO maps can be compared with the H₂S ones reported by Codella et al. (2003). In particular, Fig. 8 shows the contour maps (thin line) of the H₂S($1_{10}-1_{01}$) emission integrated over the redshifted velocity interval typical of the southern outflow: $-7, -3 \text{ km s}^{-1}$. The HDO($1_{10}-1_{01}$) map, integrated over the same velocity range, is drawn by using a thick contour. From the H₂S contours it is possible to detect the SE outflow (ending at the position of the clump A) and the southern outflow, which extends at the position of the clump C. The HDO map is in agreement with the picture given by H₂S, both suggesting an outflow activity towards South. This scenario could reflect different chemical and/or physical conditions for the regions where the different flows are moving. The southern outflow seems chemically enriched with respect to the typical gas composition of the dark clouds. It shows a redshifted component (see Fig. 6), whereas the blueshifted counterpart could be

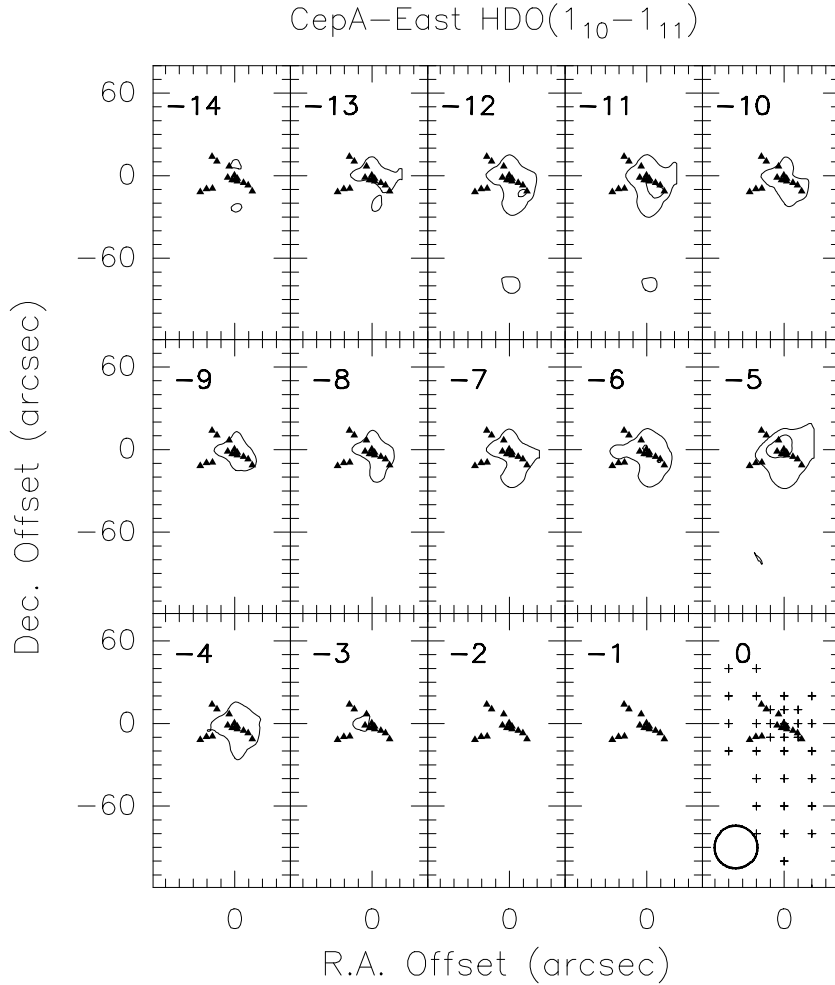


Figure 6. Channel map of the HDO $J_{K-K_+} = 1_{10}-1_{11}$ emission towards CepA-East. Each panel shows the emission integrated over a velocity interval of 1 km s^{-1} centred at the value given in the left corner. Symbols are drawn as in Fig. 1. The ambient velocity emission is -10.7 km s^{-1} according to CS $J = 5-4$ and $\text{C}^{18}\text{O } J = 2-1$ measurements (see text). The contours range are 0.03 ($\sim 3\sigma$) and 0.06 K km s^{-1} .

tentatively singled out in the emission around $\sim -12 \text{ km s}^{-1}$, i.e. at velocities close to the ambient one, but slightly blueshifted with respect to the -10.7 km s^{-1} value. In particular, the tentative detection of HDO emission at $(0'', -80'')$ shown in the channel maps in Fig. 6 is supported by the occurrence of a H_2S red- and blueshifted (see Fig. 4 of Codella et al. 2003) clump at the same position.

In Fig. 9 we summarise all the information given by the CS and HDO channel maps, drawing a schematic picture with the main clumps and outflow directions. The high excitation HDO($2_{11}-2_{12}$) line is tracing the region close to the YSOs, marked in Fig. 9 by an asterisk at $(0'', 0'')$ offset representing the HW2 coordinates. Four main flows are identified: three (SW, NE, and SE) associated with the VLA sources and probably accelerating high density material traced by CS. The SW outflow is traced also by HDO emission. In addition HDO reveals a fourth outflow pointing towards South and not traced by the VLA sources nor by the CS structures. Finally, we note that the highest HDO excitation conditions occur near the YSOs, where the beam deconvolved line intensity ratio $R_{\text{HDO}} \simeq T_{\text{mb}}(2_{11}-2_{12})/T_{\text{mb}}(1_{10}-1_{01})$ is about 2.

On the other hand, the southern flow suggests lower excitation conditions, with $R_{\text{HDO}} \simeq 0.6$ at the $(0'', -20'')$ offset.

4 A SPECTRAL SURVEY TOWARDS CEPA-EAST

Figure 10 presents the most representative examples of line profiles observed towards CepA-East. Different molecules exhibit different spectral behaviours and they can be grouped in three classes, summarised in Table 3: (i) ambient species (C^{13}CH , C_3H_2 , CH_2CO , $\text{CH}_3\text{C}_2\text{H}$, HC^{18}O^+), not detected at high velocities and with relatively narrow ($3-4 \text{ km s}^{-1}$) lines at velocities close to the ambient one (hereafter called ambient peak), (ii) outflow tracers (CO , CS , H_2S , SiO , SO , SO_2), which show extended wings (e.g. $v-v_{\text{LSR}}$ up to $\sim 30 \text{ km s}^{-1}$ for CO and 10 km s^{-1} for SO) and span the whole range of observed velocities, and (iii) species (OCS , H_2CS , HDO , and CH_3OH) which are associated with wings and, in addition, show a redshifted secondary peak at -5.5 km s^{-1} (hereafter called outflow peak), well separated (by about 5 km s^{-1}) from the ambient velocity. Unfortun-

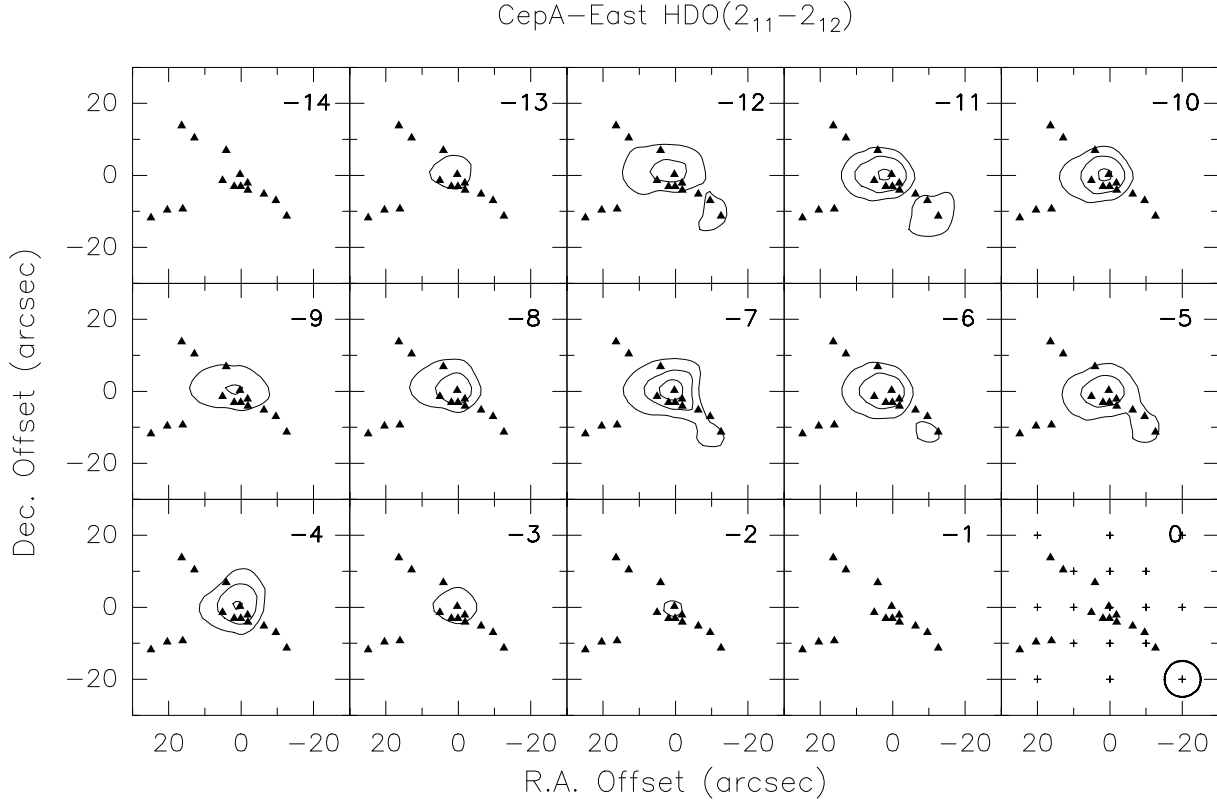


Figure 7. Zoom of the channel map of the HDO $J_{K_{-}K_{+}} = 2_{11}-2_{12}$ emission towards CepA-East. Each panel shows the emission integrated over a velocity interval of 1 km s^{-1} centred at the value given in the left corner. Symbols are drawn as in Fig. 1. The ambient velocity emission is -10.7 km s^{-1} according to CS $J = 5-4$ and $\text{C}^{18}\text{O } J = 2-1$ measurements (see text). The contours range are 0.12 ($\sim 3\sigma$), 0.24, and 0.36 K km s^{-1} .

Table 3. Summary of the properties of the profiles observed towards CepA-East

Molecular tracers in CepA-East		
CH_3OH , HCS^+ , HDO, H_2CS , OCS	\Rightarrow	Ambient, Outflow, and Peak @ -5.5 km s^{-1}
CO, CS, H_2S , SiO, SO, SO_2	\Rightarrow	Ambient and Outflow
C^{13}CH , C_3H_2 , CH_2CO , $\text{CH}_3\text{C}_2\text{H}$, HC^{18}O^+	\Rightarrow	Only Ambient

nately, the present data do not allow us to clarify the spatial distribution of the spectral outflow peak, i.e. whether it is tracing a small clump or it is related to a more extended structure. However, the comparison between HDO and H_2S emissions shown in Fig. 9 clearly suggests that the spectral outflow peak is tracing an elongated structure flowing towards South. Only accurate CH_3OH , H_2CS , and OCS maps can confirm this conclusion.

Figure 11 displays the $\text{CH}_3\text{OH}(5_K-4_K)$ and (3_K-2_K) spectra in the upper and lower panel, respectively: the dashed lines indicate the predicted positions of the hyperfine component at different excitations. Although different lines are blended, from these spectacular emissions it is possible to see that almost all the components, including those at very high excitations with $E_u \simeq 120 \text{ K}$, have been detected and show the redshifted peak. It is worth noting that other very high excitation CH_3OH lines (up to $E_u = 390 \text{ K}$) have been serendipitously detected, as reported in Table 1. Finally, Fig. 12 shows the striking differences observed on the profiles of several transitions of HDO (upper pan-

els) and H_2CS (lower panels). From these spectra, it is clear that the two HDO peaks are associated with roughly similar excitation conditions, whereas for H_2CS , the -5.5 km s^{-1} peak increases its intensity with respect to the -10.7 km s^{-1} peak with excitation indicating different physical conditions. For instance, the ratio between the mean brightness temperatures of the outflow and ambient peaks is ~ 0.6 for the $J_{K_{-}K_{+}} = 7_{16}-6_{15}$ transition at 60 K , while it is ≤ 0.1 for the $J_{K_{-}K_{+}} = 3_{13}-2_{12}$ line at 23 K .

In conclusion, the obtained line profiles indicate that at the CepA-East positions the emissions due to the clump hosting the YSOs and to the associated molecular outflows coexist and produce two distinct line peaks which suggest different excitation conditions. The results suggest also that different molecules can trace different excitation conditions at the same observed velocity. This gives us a precious opportunity to perform a multiline analysis in order to clarify the physical conditions associated with the ambient emission and those associated with the southern chemically rich molecular outflow.

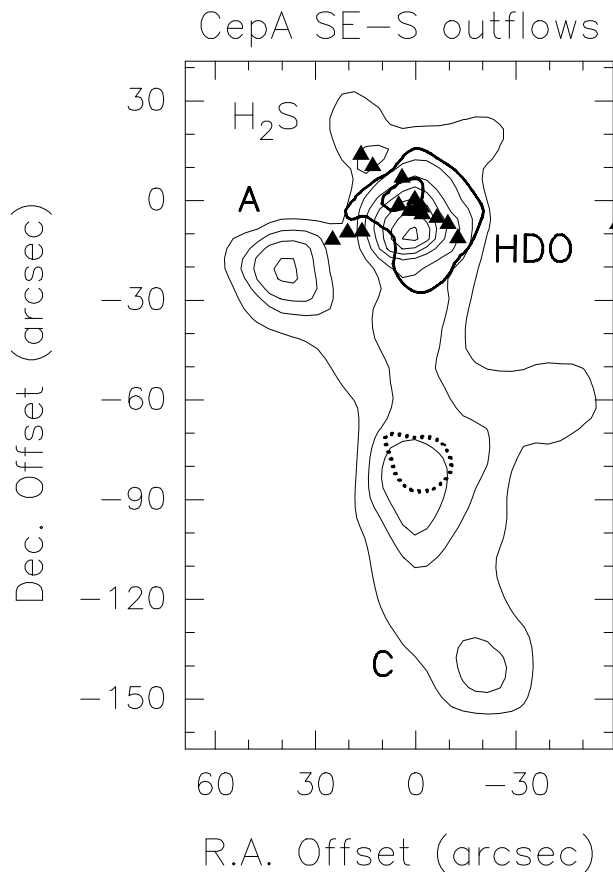


Figure 8. Contour maps (thin line) of the $\text{H}_2\text{S}(1_{10}-1_{01})$ redshifted emission (Codella et al. 2003) integrated over the velocity interval $-7, -3 \text{ km s}^{-1}$. Two main flows are clearly drawn: one pointing to SE (and ending at the clump A position), and another towards South (ending at clump C). Symbols are drawn as in Fig. 1. The thick solid line shows the contour maps of the $\text{HDO}(1_{10}-1_{01})$ emission integrated over the same range of velocity. The thick dotted line shows the distribution of the $\text{HDO}(1_{10}-1_{01})$ emission integrated over the interval $-13, -11 \text{ km s}^{-1}$ and tentatively points out a blueshifted counterpart (see the channel maps of Fig. 6).

5 DERIVED GAS PARAMETERS

5.1 Analysis procedures

By means of statistical-equilibrium calculations and using the four observed SO lines, it is possible to estimate the total column density (N_{tot}) as well as the kinetic temperature (T_k) and the hydrogen density (n_{H_2}). A Large Velocity Gradient (LVG) model and the collisional rates from Green (1994) have been used. Due to the lack of SO maps, these calculations have been performed using the mean-beam brightness temperatures relative to the intensities of the four spectra, without beam filling factor correction. If the source was definitely smaller than the four beamwidths, the LVG calculations would lead to an overestimate of the column densities (up to a factor 9) and of excitation conditions (up to factors 1.2 and 2 for T_k and n_{H_2} , respectively).

Following Cesaroni et al. (1991), statistical equilibrium computations in the LVG approximation have been used to analyse the CS and C^{34}S spectra. In particular, for optically thin conditions, the line brightness temperatures de-

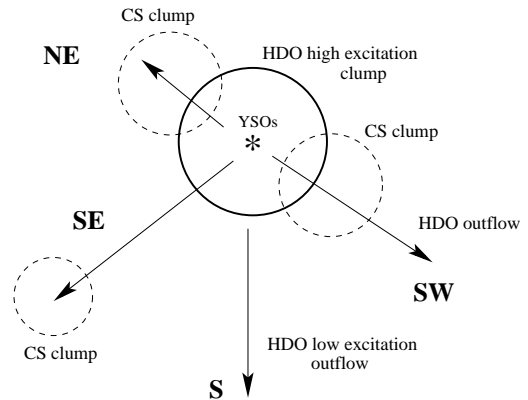


Figure 9. A schematic picture (not to scale) of the directions of the multiple outflows driven by the CepA-East YSOs as traced by HDO and CS emission (see text). Following the channel maps four main flows are identified: three (SW, NE, and SE) associated with the VLA shocked chains and with CS clumps, and one (S) traced by the $\text{HDO}(1_{10}-1_{01})$ emission. The higher excitation $\text{HDO}(2_{11}-2_{12})$ line well defines the SW outflow and with the central region close to the YSOs coordinates (marked by an asterisk).

pend only on density and, to a minor degree, on temperature. In this case, we excluded CS(2-1) which clearly shows self-absorption effects and we used CS(5-4) as well as the C^{34}S lines to derive n_{H_2} estimates.

For the CH_3OH , $\text{CH}_3\text{C}_2\text{H}$, H_2CS , and $^{34}\text{SO}_2$ molecules, observed through at least three lines, in order to estimate the rotational temperature and column densities, the standard rotation diagram method, assuming LTE and optically thin conditions, has been used. For the other molecular species, the total column densities have been calculated using the constants given in the databases for molecular spectroscopy and considering the temperature estimates derived from the LVG and rotation diagram results. For comparison, also the values calculated by using the H_2S and SO_2 emissions (Codella et al. 2003) are reported.

When possible, different column densities have been derived for the different lines at -10.7 and -5.5 km s^{-1} . In particular, the methanol patterns clearly allow us to derive different excitation conditions, while H_2CS leads to an estimate of the temperature for the -10.7 km s^{-1} component. Finally, following the SO_2 analysis of Codella et al. (2003), we have assumed two components also for CS and SO which show strong redshifted wing emission with an intense emission around -5 km s^{-1} .

5.2 Results

The derived parameters have been summarised in Table 4. The LVG results based on the SO spectra lead to kinetic temperatures of 60-100 K and $n_{\text{H}_2} \sim 5 \cdot 10^6 \text{ cm}^{-3}$ for the -10.7 km s^{-1} line at ambient velocity, while slightly higher temperatures (70-180 K) and definitely higher densities ($2 \cdot 10^6$ - $6 \cdot 10^7 \text{ cm}^{-3}$) have been derived for the -5.5 km s^{-1} component. The total SO column densities are around $4 \cdot 10^{14}$ and $5 \cdot 10^{13} \text{ cm}^{-2}$ for the ambient and outflow components, respectively.

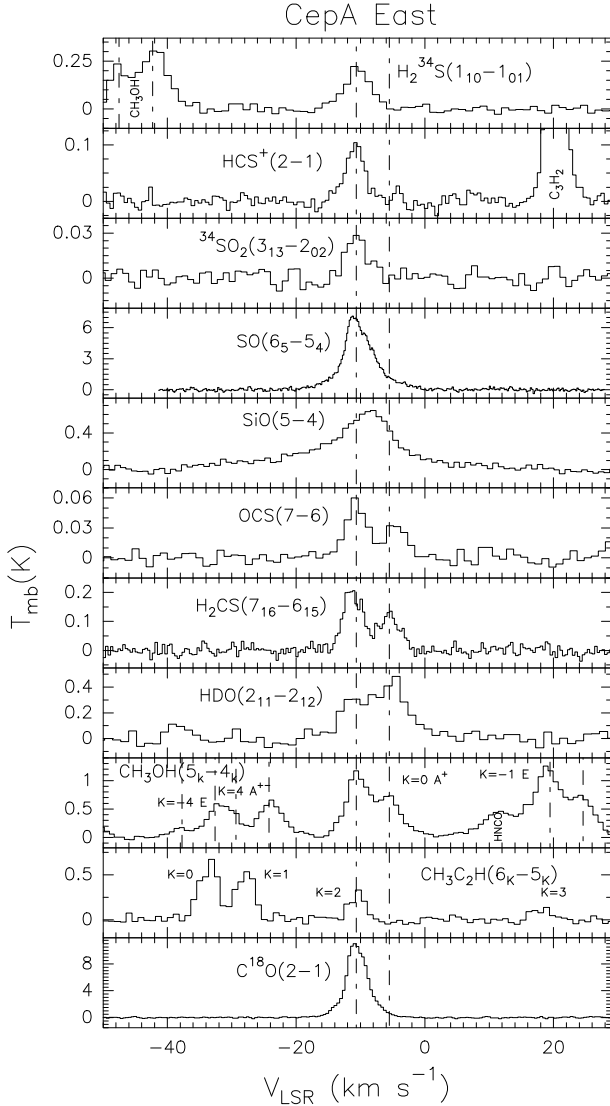


Figure 10. Molecular line profiles observed towards CepA East: species and transitions are reported. The dashed lines stand for the ambient LSR velocity (-10.65 km s^{-1}), according to the C^{18}O measurement, and for the component at -5.51 km s^{-1} well outlined e.g. in the H_2CS profile. In case of the $\text{CH}_3\text{OH}(5_K-4_K)$ spectrum, four hyperfine lines at different excitations are present: $K=0 \text{ A}^+$ ($E_u=35 \text{ K}$), $K=-1 \text{ E}$ ($E_u=39 \text{ K}$), $K=-4 \text{ E}$ ($E_u=122 \text{ K}$), and $K=4 \text{ A}^{+-}$ ($E_u=115 \text{ K}$). The $\text{CH}_3\text{C}_2\text{H}(6_K-5_K)$ pattern shows the $K=0,1,2,3$ lines. The small vertical labels CH_3OH ($E_u=126 \text{ K}$), C_3H_2 , and HNCO refers to three serendipity detections (see Table 1).

The CS LVG results indicate hydrogen number densities larger than $6 \times 10^4 \text{ cm}^{-3}$ for the ambient component. For the outflow component, the CS analysis leads to densities in the range between 4×10^3 and $5 \times 10^4 \text{ cm}^{-3}$. On the other hand, the C^{34}S data for the ambient component suggest lower densities with values around $2 \times 10^4 \text{ cm}^{-3}$. The C^{34}S emission is optically thinner than the CS one, and in fact CS shows self-absorption whereas C^{34}S shows Gaussian profiles; thus, it is reasonable to expect that C^{34}S is tracing inner regions with respect to CS. In this case, the LVG results seem to give puzzling results for CepA-East with a high density envelope and a lower density central region. One possible solution comes

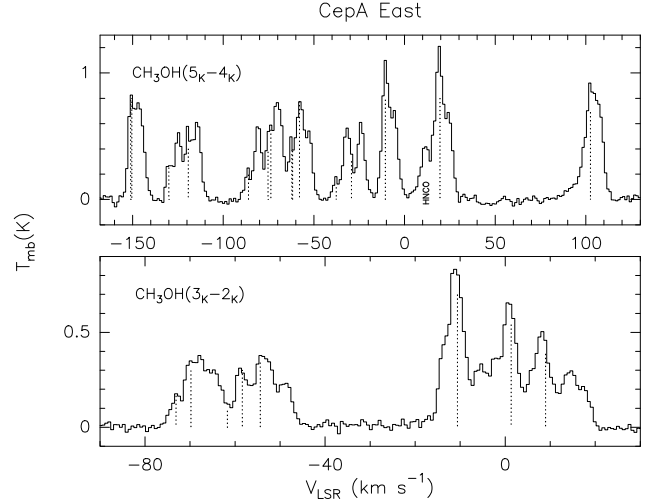


Figure 11. $\text{CH}_3\text{OH}(5_K-4_K)$ and $\text{CH}_3\text{OH}(3_K-2_K)$ line profiles observed towards CepA East. The dotted lines stand for the predicted positions of the hyperfine components at different excitations. The $\text{HNCO}(11_{011}-10_{010})$ line is also marked in the methanol (5_K-4_K) pattern. The velocity scale of the spectra is calculated with respect to the frequency of the 5_0-4_0 A^+ (241791.43 MHz) and 3_0-2_0 A^+ (145103.23 MHz) lines.

from the recent results reported by Bottinelli & Williams (2004), who analyse the large scale dynamics of CepA-East by using a density profile measured from a $850 \mu\text{m}$ map of the region. The model proposed by these authors has a high density center with depleted CS and an outer envelope with a low n_{H_2} and normal CS abundance. Therefore, our hydrogen density estimates could be biased by the fact that the CS abundance is varying along the central region.

The least-square fits to all detected lines in the CH_3OH rotation diagram, shown in Fig. 13, gives, for the ambient component (middle panel), rotational temperatures of about 30 K , while the total methanol column density is about $7 \times 10^{14} \text{ cm}^{-2}$. The CH_3OH temperature is confirmed by the $\text{CH}_3\text{C}_2\text{H}$ rotation diagram which leads to 37 K . This suggests that at the ambient velocities both molecules trace similar environments. On the other hand, for the outflow component (lower panel of Fig. 13) the derived temperature is 220 K and the CH_3OH column density is $3 \times 10^{15} \text{ cm}^{-2}$. However, due to the blending between ambient and outflow components for the methanol spectral patterns, the plot for the outflow component is less clear and the fit is definitely more doubtful. In any case, the comparison between the plots of the ambient component and the outflow one, which shows high excitation ($E_u = 390 \text{ K}$) CH_3OH emission, clearly indicates a definitely higher temperature for the outflow component.

Using the H_2CS and $^{34}\text{SO}_2$ emissions, an estimate of the rotational temperature of the ambient emission, observed in three lines, has also been obtained. The results lead to low temperatures (20 K) for H_2CS and definitely higher values (200 K) for $^{34}\text{SO}_2$, suggesting that the H_2CS spectral peak at rest velocity mainly traces relatively cool ambient material. The column densities are $N_{\text{H}_2\text{CS}} \simeq 3 \times 10^{13}$ and $N_{^{34}\text{SO}_2} \simeq 10^{14} \text{ cm}^{-2}$.

Taking into account the temperature estimates obtained from the SO and CH_3OH data, the total column densities for

Table 4. Column densities, temperatures, and hydrogen densities for the ambient and outflow gas components

Molecules	N_{tot}^a (cm^{-2})	AMBIENT			N_{tot}^a (cm^{-2})	OUTFLOW PEAK			f^b
		T_{kin} (K)	n_{H_2} (cm^{-3})	$X[\text{ }]/X[\text{H}_2]^a$		T_{kin} (K)	n_{H_2} (cm^{-3})	$X[\text{ }]/X[\text{H}_2]^a$	
C^{13}CH	$0.6\text{--}3 \times 10^{13}$	—	—	$0.2\text{--}3 \times 10^{-8c}$	—	—	—	—	—
C_3H_2	$0.6\text{--}5 \times 10^{13}$	—	—	$0.2\text{--}5 \times 10^{-10}$	—	—	—	—	—
CH_2CO	$0.3\text{--}1 \times 10^{15}$	—	—	$8 \times 10^{-10}\text{--}1 \times 10^{-8}$	—	—	—	—	—
$\text{CH}_3\text{C}_2\text{H}$	1×10^{15}	37	—	$0.3\text{--}1 \times 10^{-8}$	—	—	—	—	—
CH_3OH	7×10^{14}	33	—	$2\text{--}7 \times 10^{-9}$	3×10^{15}	220	—	6×10^{-8}	20
$\text{CO}, \text{C}^{18}\text{O}$	$1\text{--}4 \times 10^{19}$	—	—	—	5×10^{18}	—	—	—	—
$\text{CS}, \text{C}^{34}\text{S}$	$1\text{--}5 \times 10^{14}$	—	$> 6 \times 10^4$	$0.3\text{--}5 \times 10^{-9}$	3×10^{13}	—	$4 \times 10^3\text{--}5 \times 10^4$	6×10^{-10}	1
HC^{18}O^+	$1\text{--}6 \times 10^{12}$	—	—	$3 \times 10^{-8}\text{--}1 \times 10^{-10c}$	—	—	—	—	—
HCS^+	$0.3\text{--}1 \times 10^{13}$	—	—	$8 \times 10^{-12}\text{--}1 \times 10^{-10}$	3×10^{12}	—	—	6×10^{-11}	4
HDO	$2\text{--}5 \times 10^{14}$	—	—	$0.5\text{--}5 \times 10^{-9}$	6×10^{14}	—	—	1×10^{-8}	11
H_2CS	3×10^{13}	20	—	$0.8\text{--}3 \times 10^{-10}$	1×10^{14}	—	—	2×10^{-9}	16
$\text{H}_2\text{S}, \text{H}_2^{34}\text{S}^{d,e}$	5×10^{14}	27	—	$1\text{--}5 \times 10^{-9}$	--_d	--_d	--_d	--_d	--_d
HNCO	$2\text{--}3 \times 10^{13}$	—	—	$0.5\text{--}3 \times 10^{-10}$	—	—	—	—	—
OCS	$2\text{--}5 \times 10^{13}$	—	—	$0.5\text{--}5 \times 10^{-10}$	5×10^{13}	—	—	1×10^{-9}	11
SiO^d	1×10^{13}	150	2×10^6	$0.3\text{--}1 \times 10^{-10}$	--_d	--_d	--_d	--_d	--_d
SO	4×10^{14}	60–100	$4\text{--}6 \times 10^6$	$1\text{--}4 \times 10^{-9}$	5×10^{13}	70–180	$2 \times 10^6\text{--}6 \times 10^7$	1×10^{-9}	0.7
SO_2^e	3×10^{15}	75	—	$0.9\text{--}3 \times 10^{-8}$	1×10^{15}	130	—	2×10^{-8}	1.5
$^{34}\text{SO}_2$	1×10^{14}	200	—	$0.3\text{--}1 \times 10^{-9}$	—	—	—	—	—

^a The column densities and the abundances regarding the species detected through only one line have been derived assuming $X[\text{CO}]/X[\text{H}_2] = 10^{-4}$, and $T_{\text{kin}} = 20\text{--}100$ K (ambient peak) and $T_{\text{kin}} = 200$ K (outflow peak), following the temperature measurements based on the $\text{CH}_3\text{C}_2\text{H}$, CH_3OH , SO , and SO_2 emissions. ^b Average ratio between the outflow and the ambient abundances. ^c For C^{13}CH and HC^{18}O^+ , the abundances refer to the most abundant isotopomers (CCH and HCO^+) calculated by assuming $^{12}\text{C}/^{13}\text{C} = 89$ and $^{16}\text{O}/^{18}\text{O} = 490$ (Wilson & Rood 1994). ^d For H_2S and SiO the ambient and outflow components cannot be disentangled; thus the values refer to the whole emission and the abundances are not reported. ^e The H_2S and SO_2 results are taken from the Codella et al. (2003) paper: the H_2^{34}S emission has been used to derive the optical depth and consequently refine the H_2S column density.

the molecular species observed in one or two lines have been calculated using the spectroscopic constants given in the literature and summarised in the JPL (Pickett et al. 1998), NIST (Lovas 2004), Cologne (Müller et al. 2001), and Leiden (Schöier et al. 2005) databases and considering a kinetic temperature in the range 20–100 K for the ambient component and 200 K for the outflow one. Table 4 reports the values of the total column densities for the ambient emission: $N_{\text{C}^{13}\text{CH}}$ and $N_{\text{C}_3\text{H}_2}$ are about $1 \times 10^{14} \text{ cm}^{-2}$, N_{HNCO} and $N_{\text{OCS}} \simeq 3 \times 10^{13} \text{ cm}^{-2}$, $N_{\text{CH}_2\text{CO}} \sim 5 \times 10^{15} \text{ cm}^{-2}$, $N_{\text{HC}^{18}\text{O}^+}$ and $N_{\text{HCS}^+} \sim 3\text{--}5 \times 10^{12} \text{ cm}^{-2}$, while N_{HDO} is around $3 \times 10^{14} \text{ cm}^{-2}$. On the other hand, for the outflow component we have column densities around 3×10^{12} , 6×10^{14} , and $5 \times 10^{13} \text{ cm}^{-2}$ for HCS^+ , HDO , and OCS , respectively. We note that the HCS^+/CS abundance ratio is quite large, ~ 0.1 , in the outflow peak, close to that measured in dark clouds (Ohishi et al. 1992), suggesting that the HCS^+ emission has been overestimated, due the low S/N ratio of the HCS^+ outflow peak, and/or that the derived CS abundance is underestimated, probably due to the blending between ambient and outflow spectral components (Sect. 5.1).

The SiO results shown in Table 4 refer to the multiline SiO survey given by Codella et al. (1999), whereas the H_2S and SO_2 results are taken from the Codella et al. (2003) paper: the H_2^{34}S emission have been used here to derive the optical depth, $\tau_{(1_{10}-1_{01})} \simeq 1\text{--}2$, and consequently refine the H_2S column density. Finally, it is worth noting that for H_2S and SiO the ambient and outflow components cannot be disentangled both showing continuous extended wings, and thus the values in Table 4 refer to the whole emission.

In conclusion, we find that in CepA-East at ambient velocities (i) the gas is associated with high densities, $> 10^5 \text{ cm}^{-3}$, and (ii) different components at different temperatures coexist, ranging from the relatively low kinetic temperatures, less than 50 K, measured with H_2S , CH_3OH , H_2CS , and $\text{CH}_3\text{C}_2\text{H}$, to definitely higher temperature conditions, $\sim 100\text{--}200$ K, obtained from the SiO , SO , and SO_2 spectra. In other words, at ambient velocities we are probably sampling different layers of the high-density medium hosting the star forming process, some of them probably heated by the stellar radiation. On the other hand, for the outflow component we derive two density regimes: about 10^4 cm^{-3} from CS and around 10^7 cm^{-3} from SO, whereas the temperatures are always quite high: $\simeq 100\text{--}200$ K, indicating regions compressed and heated by shocks.

6 DISCUSSION

6.1 Abundances

With the aim of obtaining an estimate of the abundances of the observed species, the H_2 column densities have been derived from C^{18}O for the ambient component and from CO and C^{18}O for the outflow peak, by assuming a standard $X[\text{CO}]/X[\text{H}_2]$ ratio ($\simeq 10^{-4}$; Frerking et al. 1982, Lacy et al. 1994). We obtained the fractional abundances with respect to H_2 as the ratio between column densities and finally an enhancement factor f for each molecule has been derived as the ratio between the abundances in the outflow and in the ambient peaks. The derived values are reported in the last

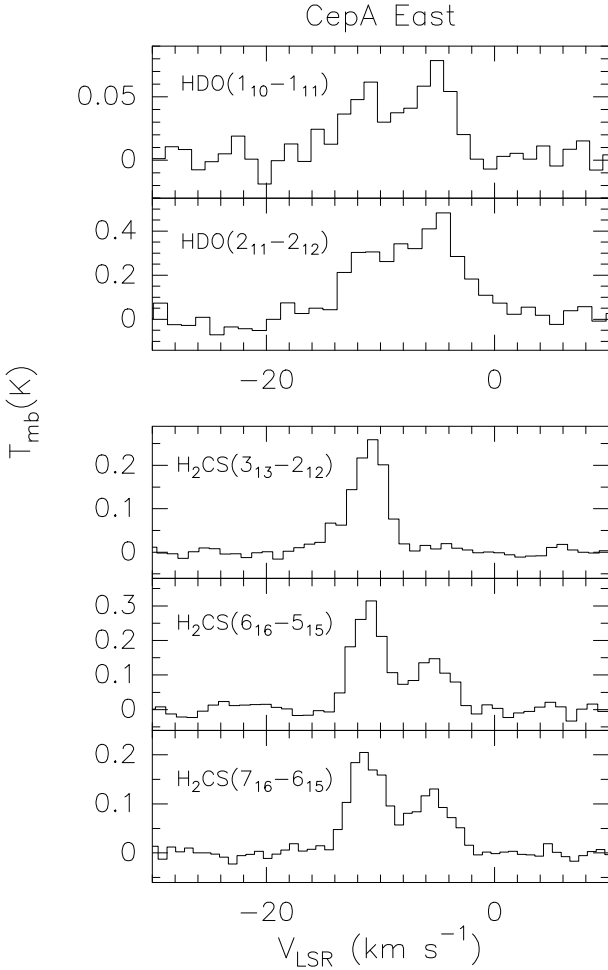


Figure 12. HDO (upper panels) and H₂CS (lower panels) line profiles observed towards CepA East: transitions are reported (see Table 1). Note how for H₂CS the -5.5 km s^{-1} component increases its intensity with respect the -10.7 km s^{-1} peak with excitation.

column of Table 4, where two classes can be distinguished. On the one hand, CS, SO, and SO₂ do not show a definite abundance enhancement ($f \simeq 1$), while the HCS⁺ abundance increases only by a factor of 4. On the other hand, CH₃OH, HDO, H₂CS, and OCS appear to be definitely enhanced by at least one order of magnitude ($f \sim 10\text{--}20$), confirming that these molecules are closely associated with the chemistry occurring in molecular outflows (Bachiller & Pérez Gutiérrez 1999).

Given the well known observational difficulties of detecting the H₂O isotopomer, HDO represents with H₂¹⁸O an alternative tool to investigate the occurrence of water emission in space. In fact, HDO has been already observed towards high-mass star forming regions, mainly hot cores (e.g. Jacq et al. 1990, Helmich et al. 1996, Gensheimer et al. 1996 and references therein). In addition, the high velocity peak indicates that HDO, and thus water, is a very sensitive shock tracer in molecular outflows driven by YSOs. The present data do not allow us to give a direct estimate of the H₂O abundance. However, by assuming the cosmic [D]/[H] ratio, $\sim 1.5 \cdot 10^{-5}$ (Oliveira et al. 2003), or the typical [D]/[H] ratios derived for hot cores, $2\text{--}6 \cdot 10^{-4}$ (Jacq et al. 1990),

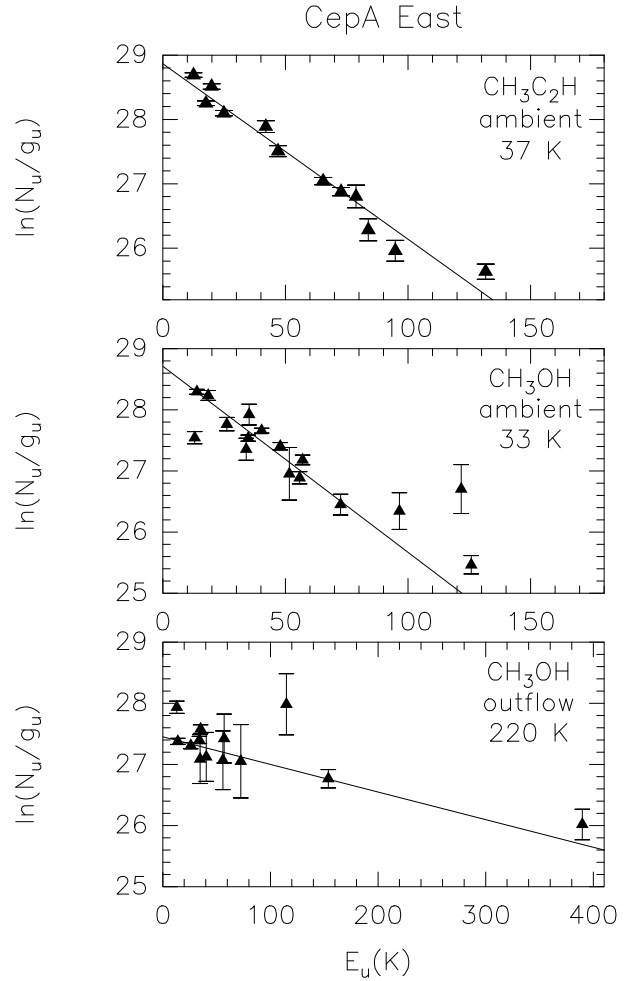


Figure 13. Rotation diagrams for the CH₃C₂H (upper panel) and CH₃OH (middle and lower panels) transitions measured towards CepA-East. For the methanol emission two spectral regimes have been considered: ambient and outflow (see text). The parameters N_u , g_u , and E_u are, respectively, the column density, the degeneracy and the energy for the upper levels of the transitions reported. The derived values of the rotational temperature are reported.

it is possible to roughly calculate a H₂O abundance from our HDO measurements. We therefore derive for CepA-East $X[\text{H}_2\text{O}]/X[\text{H}_2]$ in the $10^{-6}\text{--}10^{-4}$ range for the ambient peak and $\simeq 10^{-5}\text{--}10^{-4}$ for the outflow peak, confirming that the water abundance can be extremely enhanced in star forming regions and that H₂O is a major coolant in warm gas (van Dishoeck & Blake 1998 and references therein).

Finally, the high abundances of CH₃OH, HDO, H₂CS, and OCS, which show a well separated high velocity range (see Figs. 10 and 12), are useful tools to investigate the shocked material by comparing to those of other shock tracers such as SiO, SO, and SO₂.

6.2 Different tracers at different velocities

In order to investigate the properties of the line wings which do not show the peak at -5.5 km s^{-1} , Fig. 14 reports the distribution with velocity of the brightness temperature ratio between SO(7–6) (upper panel), SO₂(5₂₄–4₁₃) (middle

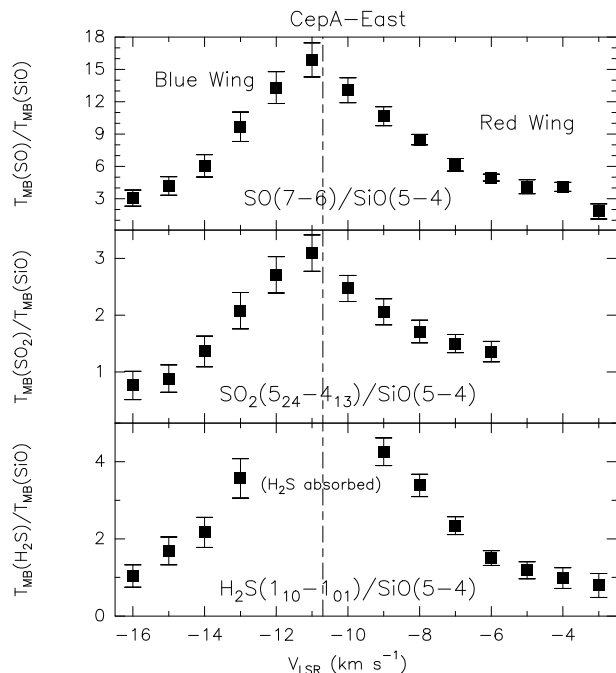


Figure 14. Distribution with velocity of the ratio between the brightness temperatures of the SO(7–6) ($E_u = 35$ K; upper panel), H₂S(1₁₀–1₀₁) ($E_u = 28$ K; middle panel), SO₂(5₂₄–4₁₃) ($E_u = 24$ K; lower panel) lines and of the SiO(5–4) ($E_u = 21$ K) profile as detected towards CepA-East. The H₂S and SO₂ data are taken from Codella et al. (2003). The HPBW of the observations used here are: 9'' (SO), 10'' (SO₂), and 11'' (H₂S, SiO). The dot-dashed line underlines the ambient LSR velocity according to the CS $J = 5-4$ and C¹⁸O $J = 2-1$ measurement.

panel), H₂S(1₁₀–1₀₁) (lower panel) and SiO(5–4), as observed towards CepA-East. Note that for such a comparison we selected transitions observed with a similar HPBW (SO: 9'', SO₂: 10'', H₂S and SiO: 11'') and with similar excitation ($E_u \sim 21-35$ K, see Table 1). From Fig. 14 it is possible to see that:

(i) SiO emission dominates at the largest velocities, where the highest excitation conditions are expected. Actually, a comparison between the line profiles of different excitation transitions of H₂S and SO₂ observed towards CepA-East clearly indicates that the higher the velocity the higher the excitation (see Fig. 8 of Codella et al. 2003);

(ii) among the S-bearing species, SO₂ has the distribution associated with the largest width, followed by SO, and finally by H₂S. This is confirmed also by the SO/H₂S, SO₂/H₂S, and SO₂/SO column density ratio profiles, not shown here, which increase with velocity.

These results confirm the close association of SiO with the shocks occurring along the molecular outflows. Sputtering on dust grains is probably the most efficient mechanism that leads to a SiO abundance enhancement, although also grain-grain collisions can play a role depending on the gas density (Schilke et al. 1997, Caselli et al. 1997). However, it seems that H₂S, SO, and SO₂ preferentially trace more quiescent regions than SiO. From the different widths of the resultant column density ratio profiles, we note the lack of an intense H₂S emission at the highest velocities. A possible explanation is a fast conversion of H₂S into SO and SO₂

and possibly OCS, in agreement with the chemical models where first H₂S is injected from grains, then the other S-bearing species are formed very quickly in $\sim 10^3$ yr (Pineau des Forêts et al. 1993, Charnley 1997, Viti et al. 2004). Alternatively, it may be that hydrogen sulphide is not the major sulphur carrier in the grain mantles, as suggested also by the lack of H₂S features in the ISO spectra (Gibb et al. 2000, Boogert et al. 2000) and by the low temperature derived from the present H₂S spectra, ~ 27 K, well in agreement with that measured by van der Tak et al. (2003, 25 K) towards high-mass star forming regions.

On the other hand, the occurrence of the outflow peak at -5.5 km s⁻¹ shows that:

(i) OCS and H₂CS emit at high velocities, where SiO emission starts to dominate and the excitation conditions are high. At these velocities also the abundance of CH₃OH, which is expected to be abundant in grain mantles and to be released in the gas phase after shocks, definitely increases. These results suggest that OCS and H₂CS are among the sulphur carriers in the grain mantles, or that at least they are rapidly formed once the mantle is evaporated. Both scenarios are in agreement with the results by van der Tak et al. (2003) who measured high excitation temperatures for OCS (~ 100 K). Unfortunately, the present data do not allow us to derive a direct temperature estimate from the OCS data. However, an estimate of the temperature of the gas traced by OCS is given by the CH₃OH emission, which well defines the OCS outflow peak and leads to a high temperature: 220 K;

(ii) HDO shows an enhancement of its fractional abundance ($X[\text{HDO}]/X[\text{H}_2]$) at such high velocities. From the estimated value, 10^{-8} , we can roughly infer the abundance of water assuming a D/H ratio equal to $1.5 \cdot 10^{-5}$ (Oliveira et al. 2003): $X[\text{H}_2\text{O}]/X[\text{H}_2] \simeq 6 \cdot 10^{-4}$. This suggests that the majority of oxygen is here locked into water molecules (Meyer et al. 1998). This is expected if we are observing regions heated by shocks above 200 K, so that the majority of OH molecules quickly produce water through reactions with molecular hydrogen (e.g. Hartquist et al. 1980). The methanol measurements confirm the occurrence of high temperatures at these velocities.

Finally, note that sulphur could be also in atomic form when evaporated from the grain mantles, as suggested by Wakelam et al. (2004). However, the atomic S is expected to be very quickly ($\leq 10^3$ yr) locked into SO and SO₂, so that a big amount of atomic S is not expected to last in the gas phase for a long time and thus difficult to observe. The form that sulphur takes on dust grains is still far to be known: the present data indicate that OCS and H₂CS may play an important role and/or that they are effectively formed in high-temperature gas.

In conclusion, the present analysis of the line profiles indicates that H₂S, SO, and SO₂ may not be easily used as chemical clocks of the shocked material. On the other hand, H₂CS and OCS could be useful candidates: in the next section, a possible use of their emission is discussed.

6.3 On the origin of the outflow spectral peak

Since the outflow peak is clearly defined by two sulphuretted species like OCS and H₂CS and by two shock tracers

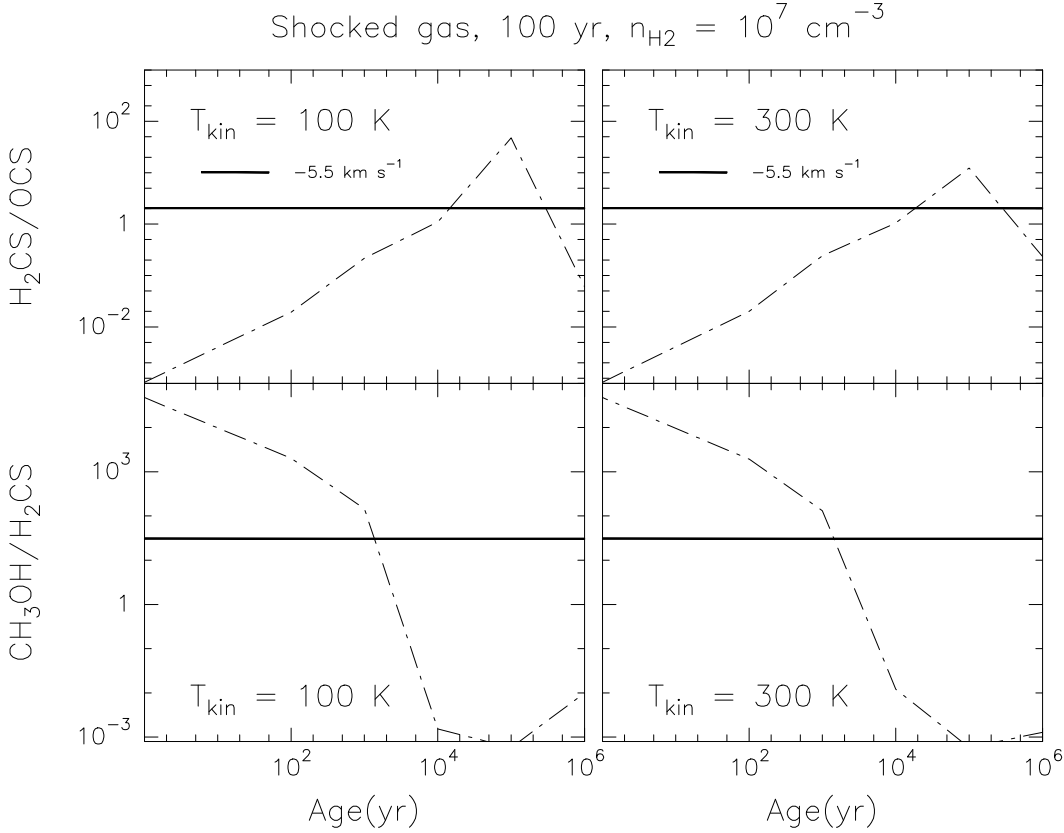


Figure 15. Evolution of the abundance ratios $\text{H}_2\text{CS}/\text{OCS}$ (upper panels) and $\text{CH}_3\text{OH}/\text{H}_2\text{CS}$ (lower panels) as functions of time for a gas shocked for 100 yr (see text), a gas density of 10^7 cm^{-3} , and gas temperatures of 100 (left panels) and 300 K (right panels), according to the Wakelam et al. (2004) model. The horizontal thick lines indicate the values derived from the observations towards CepA-East for the -5.5 km s^{-1} peak (2 for $\text{H}_2\text{CS}/\text{OCS}$ and 30 for $\text{CH}_3\text{OH}/\text{H}_2\text{CS}$, see Table 4).

like CH_3OH and HDO , we attempt to use such emission as a chemical clock. We compared the observations with the theoretical calculations recently reported by Wakelam et al. (2004). The authors developed a time-dependent chemical model of sulphur chemistry in hot-cores with up-to-date reaction rate coefficients, following the molecular composition after the injection of grain mantle species into the gas phase. They found that the abundances of the main S-bearing species (H_2S , SO , OCS , and SO_2) strongly depend on the physical conditions, on the oxygen abundance in the gas phase, on the adopted grain mantle composition as well as on the time. Hence, the use of the abundance ratios can be often useless to derive age estimates. Nevertheless, Wakelam et al. (2004) compared the observed and predicted abundance ratios for the hot cores Orion KL and IRAS16293-2422, for which the physical conditions had been previously obtained. The authors were able to reproduce the observed abundance and give an age estimate only assuming that a large amount of atomic sulphur is initially present in the post-evaporative gas, with $X[\text{S}]/X[\text{H}_2]$ between 3×10^{-5} and 3×10^{-6} .

In view of these results, we applied the Wakelam et al. (2004) model to the observed emission of the CepA outflow peak. Although the model has been initially used to investigate hot cores, it follows how the S-bearing molecular abundances vary with time when the gas undergoes a sudden change in its temperature and density, and in its

overall chemical abundance, because of the evaporation of grain mantles. Therefore, in principle, the model can be reasonably used also for shocked conditions occurring along a molecular outflow. However, the physical conditions and the evolution with time should be different from the hot core case since the physical processes are different. Magneto-Hydrodynamics models predict that during the passage of a shock wave, the gas temperature and density simultaneously increase before decreasing after the shock passage on time scales which depend on the considered model (e.g. Bergin et al. 1998, Flower & Pineau des Forêts 2003). In our cases, the physical conditions are difficult to constrain in the shocked regions because we do not know how the physical conditions evolved and also because the observed molecules indicates temperature and density ranges (see Table 4). For these reasons, we considered three different models. In the first two models, the temperature and the density suddenly increase to 1000 K and 10^7 cm^{-3} and the chemistry evolves for 100 (Case 1) and 1000 yr (Case 2), respectively. After the passage of the shock, the temperature decreases to the observed values, i.e. $\simeq 200 \text{ K}$. The chemistry of the post-shocked gas then evolves for 10^6 yr . In the third model (Case 3), we assumed that the observed molecules mostly trace the outer material of the shock where the temperature and the density only increase to the observed values without passing through a phase with temperatures around 1000 K. This last scenario is motivated by the fact that at the CepA distance (725 pc),

the filling factor relative to the shocked regions where the temperature is expected to exceed 1000 K could be definitely small and thus their emission could be strongly diluted.

From a chemical point of view, the starting point is the dark molecular cloud composition computed by the chemical model (see details of composition A in Wakelam et al. 2004). Due to the shock passage, the molecules contained on the grain mantles, such as H_2O , H_2CO , CH_3OH and S-bearing species, are sputtered in the gas phase. For the other species, we took the abundances observed as icy features towards massive star forming regions (see Wakelam et al. 2004).

Since the initial form and abundance of sulphur sputtered from grains is still an open question, as a first step, we decided to use the results of Wakelam et al. (2004) who reproduce reasonably well the S-bearing observations towards hot cores using a model in which sulphur is mainly evaporated from grains in atomic, OCS, and H_2S forms. The initial fractional abundances are 10^{-7} for OCS and H_2S , 3×10^{-6} for the S form (Palumbo et al. 1997, van Dishoeck & Blake 1998, Wakelam et al. 2004). The implicit assumption here is that the majority of sulphur is depleted in the refractory grain cores.

Since HDO is not included in the Wakelam et al. (2004) model, we only used the abundance ratios between CH_3OH , OCS, and H_2CS . Figure 15 reports the evolution of the $\text{H}_2\text{CS}/\text{OCS}$ (upper panels) and $\text{CH}_3\text{OH}/\text{H}_2\text{CS}$ (lower panels) ratios as a function of time for the Case 1 (shocked gas 100 yr old). The initial abundances of the three species are 9.8×10^{-8} , 8.20×10^{-11} , and 3.9×10^{-6} , for OCS, H_2CS , and CH_3OH , respectively. Following the physical parameters derived for the outflow peak (see Table 4) and adopting a conservative approach, we used temperatures of 100 K (left panels) and 300 K (right panels), whereas for the hydrogen density we assumed 10^7 cm^{-3} (dot-dashed line). The horizontal thick lines indicate the values derived from the observations towards CepA-East for the -5.5 km s^{-1} peak: 2 for $\text{H}_2\text{CS}/\text{OCS}$ and 30 for $\text{CH}_3\text{OH}/\text{H}_2\text{CS}$. Figure 15 shows that, for the assumed n_{H_2} and T_{kin} ranges, the observed ratios lead to ages for the shocked gas in the CepA-East redshifted component in the range $\sim 10^3$ – 3×10^4 yr. The $\text{H}_2\text{CS}/\text{OCS}$ trend is due to a maximum of the H_2CS abundance at 10^4 yr and to a decrease of the OCS abundance after 10^3 yr. On the other hand, the $\text{CH}_3\text{OH}/\text{H}_2\text{CS}$ trend is due to a dramatic decrease of the methanol abundance for ages $\geq 10^4$ yr. Note that the $\text{CH}_3\text{OH}/\text{H}_2\text{CS}$ result solves the dichotomy given by the $\text{H}_2\text{CS}/\text{OCS}$ ratio, which is less selective, proposing ages either $\leq 10^4$ yr or $\sim 10^6$ yr.

Cases 2 and 3 (shocked gas 1000 yr and warmed dark cloud) do not show significant changes and thus lead to the same conclusion, leaving open the question about the origin of the outflow peak: gas which passed through a hot phase or warm gas in the shock surroundings? In any case, even taking into account all the uncertainties of the column density estimates, of the abundance ratios, and of the physical conditions, the comparison between the observations and the model used here allow us to obtain an age for the shocked gas in CepA-East of the order of $\sim 10^3$ – 3×10^4 yr. Only precise measurements of density and temperature, which are usually hampered by the high degree of confusion associated with the observed regions, can refine age estimates further. Future investigations of emission due to S-bearing species towards other molecular outflows and

hot cores where the physical conditions are known will confirm whether the $\text{CH}_3\text{OH}/\text{H}_2\text{CS}$ and $\text{H}_2\text{CS}/\text{OCS}$ abundance ratios can in fact be used to estimate ages.

7 SUMMARY

The CepA star forming region has been investigated through a multiline survey at mm-wavelengths. The results indicate the occurrence of a rich chemistry surrounding the YSOs of the CepA-East stellar association. The main findings are as follows:

1. The CS and HDO maps draw a complex scenario, detecting high excitation clumps hosting the YSOs driving multiple outflows. Four main flows have been identified: three are along the SW, NE, and SE directions, traced also by strings of VLA continuum sources, and are accelerating high density CS clumps. In addition, HDO reveals a fourth outflow pointing towards South, which had been previously detected only through H_2S and SO_2 observations, and is then associated with conditions particularly favourable to a chemical enrichment.

2. At the CepA-East position different molecules exhibit different spectral behaviours: three classes can be identified. Some species (C^{13}CH , C_3H_2 , CH_2CO , $\text{CH}_3\text{C}_2\text{H}$, HC^{18}O^+) peak with relatively narrow lines at ambient velocities (ambient peak). Other molecules (CO , CS , H_2S , SiO , SO , SO_2) show extended wings and trace the whole range of the outflow velocities. Moreover, there is a group of species (OCS , H_2CS , HDO, and CH_3OH) which shows wings and, in addition, well defines a high velocity redshifted spectral peak (outflow peak) which can be used to investigate the SE-S outflows.

3. The physical conditions associated with both the ambient and outflow peaks have been estimated. By means of statistical-equilibrium calculations, using LVG codes, we have obtained the physical parameters of the molecular gas traced by SO and CS. For $\text{CH}_3\text{C}_2\text{H}$, H_2CS , $^{34}\text{SO}_2$, and CH_3OH we have used the rotation diagram method. For the other molecular species, we have calculated the total column densities assuming LTE conditions. At ambient velocities the gas is quite dense ($> 10^5 \text{ cm}^{-3}$) and different components at different temperatures coexist, ranging from the relatively low kinetic temperatures (≤ 50 K) measured with H_2S , CH_3OH , H_2CS , and $\text{CH}_3\text{C}_2\text{H}$, to definitely higher temperature conditions, ~ 100 – 200 K, obtained from the SiO, SO, and SO_2 spectra, which may trace layers directly heated by the stellar radiation. For the outflow component densities between $\sim 10^4 \text{ cm}^{-3}$ to $\sim 10^7 \text{ cm}^{-3}$ and high temperatures, $\simeq 100$ – 200 K, have been found, indicating regions compressed and heated by shocks.

4. The comparison between the line profiles of different outflow tracers of molecular outflows shows that SiO dominates at the highest velocities, where the highest excitation conditions are found. This confirms the close association of SiO with shocks. On the other hand, H_2S , SO_2 , and SO preferentially trace more quiescent regions. In particular, we find a lack of a bright H_2S emission at the highest velocities. Moreover, OCS and H_2CS emit at quite high velocities, where (i) SiO emission dominates and the excitation conditions are high, and (ii) CH_3OH and HDO, other shock

tracers, increase their abundance. These results could indicate that H₂S is not the only major sulphur carrier in the grain mantles, and that OCS and H₂CS may probably play an important role on the grains; or that alternatively they could rapidly form once the mantle is evaporated after the passage of a shock.

5. We checked the possible use of the CH₃OH, OCS, and H₂CS emission as chemical clocks to measure the age of the shocked material associated with the outflow peak. The observations have been compared with the theoretical calculations recently reported by Wakelam et al. (2004), who developed a time-dependent model with up-to-date reaction rate coefficients for the sulphur chemistry. Once associated with the derived physical parameters, the H₂CS/OCS and CH₃OH/H₂CS column density ratios led to ages in the range 10³-3 10⁴ yr. Further observations of emission due to sulphuretted molecules as well as accurate measurements of density and temperatures associated with the outflowing material are necessary in order to calibrate these chemical clocks.

ACKNOWLEDGEMENTS

We are grateful to J. Santiago Garcia, M. Tafalla, C. M. Walmsley, and D. A. Williams for helpful suggestions and discussions. SV acknowledges individual financial support from a PPARC Advanced Fellowship. We also thank the referee for the contribution to the improvement of the paper.

REFERENCES

- Bachiller R., Peréz Gutiérrez M., 1999, *ApJ* 487, L93
 Bachiller R., Peréz Gutiérrez M., Kumar M.S.N., Tafalla M., 2001, *A&A* 372, 899
 Bergin E.A., Melnik G.J., Neufeld D.A., 1998, *ApJ* 499, 777
 Bergin E.A., Ungerechts H., Goldsmith P.F., et al., 1997, *ApJ* 482, 267
 Boogert A.C.A., Tielens A.G.G.M., Ceccarelli C., et al., 2000, *A&A* 360, 683
 Bottinelli S., Williams J.P., 2004, *A&A* 421, 1113
 Buckle J.V., Fuller G.A., 2003, *A&A* 399, 567
 Caselli P., Hartquist T.W., Havnes O., 1997, *A&A* 322, 296
 Cesaroni R., Walmsley C.M., Kömpe C., Churchwell E., 1991, *A&A* 252, 278
 Charnley S.B., 1997, *ApJ* 481, 386
 Codella C., Bachiller R., 1999, *A&A* 350, 659
 Codella C., Bachiller R., Reipurth B., 1999, *A&A* 343, 585
 Codella C., Bachiller R., Benedettini M., Caselli P., 2003, *MNRAS* 341, 707
 Flower D.R., Pineau des Forêts G., 2003, *MNRAS* 343, 390
 Frerking M.A., Langer W.D., Wilson R. W., 1982, *ApJ* 262, 590
 Garay G., Ramírez S., Rodríguez L.F., Curiel S., Torrelles J.M., 1996, *ApJ* 459, 193
 Gensheimer P.D., Mauersberger R., Wilson T.L., 1996, *A&A* 314, 281
 Gibb E.L., Whittet D.C.B., Schutte W.A., et al., 2000, *ApJ* 536, 347
 Goetz J.A., Pipher J.L., Forrest W.J., et al., *ApJ* 504, 359
 Green S., 1994, *ApJ* 434, 188
 Hartquist T.W., Oppenheimer M., Dalgarno A., 1980, *ApJ* 236, 182
 Hatchell J., Thompson M.A., Millar T.J., Macdonald G.H., 1998, *A&A* 338, 713
 Helmich F.P., van Dishoeck E.F., Jansen D.J., 1996, *A&A* 313, 657
 Jacq T., Walmsley C.M., Henkel C., Baudry A., Mauersberger R., Jewell, P.R., 1990, *A&A* 228, 447
 Kaufman N.J., Neufeld D.A., 1996, *ApJ* 456, 250
 Lacy J.H., Knacke R., Geballe T.R., Tokunaga A.T., 1994, *ApJ* 428, L69
 Lovas F.J., 2004, *J. Phys. Chem. Ref. Data* 33, 177
 Meyer D.M., Jura M., Cardelli J.A., 1998, *ApJ* 493, 222
 Müller H.S.P., Thorwirth S., Roth D.A., Winnewisser G., 2001, *A&A* 370, L49
 Narayanan G., Walker C.K., 1996, *ApJ* 466, 844
 Ohishi M., Irvine W., Kaifu N., 1992, in *Astrochemistry of cosmic phenomena*, Proc. of the 150th Symp. of the International Astronomical Union, held at Campos do Jordao, Sao Paulo, Brasil, August 5-9, 1991, ed. P.D. Singh (Dordrecht: Kluwer), 171
 Oliveira C.M., Hébrard G., Howk J.C., Kruk J.W., Chayer P., Moos H.W., 2003, *ApJ* 587, 235
 Palumbo M.E., Geballe T.R., Tielens, A.G.G.M., 1997, *ApJ* 479, 839
 Pickett H.M., Poynter R.L., Cohen E.A., et al., 1998, *J. Quant. Spectrosc. & Rad. Transfer* 60, 883
 Pineau des Forêts G., Roueff E., Schilke P., Flower D.R., 1993, *MNRAS* 262, 915
 Sargent A.I., 1977, *ApJ* 466, 844
 Schilke P., Walmsley C.M., Pineau des Forêts G., Flower D.R., 1997, *A&A* 321, 293
 Schöier F.L., van der Tak F.F.S., van Dishoeck E.F., Black J.H., 2005, *A&A* 432, 369
 van der Tak F.F.S., Boonman A.M.S., Braakman R., van Dishoeck E.F., 2003, *A&A* 412, 133
 van Dishoeck E.F., Blake G.A., 1998, *ARA&A* 36, 317
 Viti S., Collings M.P., Dever J.W., McCoustra M.R.S., Williams D.A., 2004, *MNRAS* 354, 1141
 Wakelam V., Caselli P., Herbst E., Ceccarelli C., Castets A., 2004, *A&A* 422, 159
 Wilson T.L., Rood R.T., 1994, *ARA&A* 32, 191